J Mater Sci (2007) 42:8088–8092
DOI 10.1007/s10853-007-1678-7

Surface equilibrium angle for anisotropic grain growth in SnO_2 systems

Sergio M. Tebcherani · Sergio Cava · José A. Varela · Edson R. Leite · Elson Longo

Received: 4 May 2006 / Accepted: 9 March 2007 / Published online: 22 June 2007

Abstract Usually, the kinetic models used in the study of sintered ceramic are performed by means of indirect physical tests, such as, results obtained from data of linear shrinkage and mass loss. This fact is justified by the difficulty in the determinations of intrinsic parameters of ceramic materials along every sintering process. In this way, the technique of atomic force microscopy (AFM) was used in order to determine the importance and the evolution of the dihedral angle in the sintering of 0.5 mol% MnO_2-doped tin dioxide obtained by the polymeric precursor method.

Introduction

Experimentally, the most common way to investigate the relative energy of the grain boundary consist in establishing a relationship of the surface free energy of the material with its grains geometry [1–3]. This relationship was firstly quantified by Herring [4] who found out that the surface free energy is stationary when the balance process is reached. In this way, it is possible to determine the whole interface energy by observing the geometry of a certain number of interfaces among crystals of well-known orientation.

Thus, the flow of atoms j_a of a system is related to the intrinsic diffusion coefficient D and the gradient of chemical potential difference between the atom and the vacancy, in accordance with the Herring equation [5].

$$j_a = -\frac{D}{\Omega_a k_B T}\nabla(\mu_a - \mu_v) \tag{1}$$

where $\frac{D}{k_B T}$ represent the relative term of material mobility through the grain boundary or diffusion by the lattice, k_B is the Boltzman constant, T is an absolute temperature, Ω_a is the atomic volume, μ_a and μ_v are the chemical potentials of atom and vacancies, $\nabla(\mu_a - \mu_v)$ is the gradient between the chemical potentials difference that leads to the mass transport.

In a general way, Hansen [6] has obtained a relationship denominated as a flow general equation:

$$j_{as} = \frac{D}{k_B T}\left(\frac{\alpha\gamma C_k}{C_\lambda G^2}\right) \tag{2}$$

where α is a proportionality constant that relates the gradient with λ and is just dependent of the three-dimensional geometric relationship between sources and material drains along the limit of the grain boundary, being λ the linear average distance of defined diffusion for the intersection between a pore and the center of the neck among two grains, γ is the surface energy, G is the average grain diameter, C_k and C_λ are geometric proportionality constants where K defines the medium curvature of pore.

In surface techniques, the excess of the grain boundary free energy per surface free energy (γ_{gb}/γ_S) [7–12] is a

S. M. Tebcherani · S. Cava (✉)
Laboratório Interdisciplinar de Materiais Cerâmicos, Centro Interdisciplinar de Pesquisa e Pós-Graduação, Universidade Estadual de Ponta Grossa, Av. Gal. Carlos Cavalcanti, 4748, Campus - Uvaranas, CEP 84035-900 Ponta Grossa, PR, Brazil
e-mail: cava@uepg.br

J. A. Varela · E. R. Leite · E. Longo
Laboratório Interdisciplinar em Cerâmica, Departamento de Físico-Química, Instituto de Química, Universidade Estadual Paulista, R. Francisco Degni, s/n, Bairro Quitandinha, CEP 14800-900 Araraquara, SP, Brazil

function of the dihedral angle of experimental surface measured by the intersection Ψ_S giving the equation:

$$\frac{\gamma_{gb}}{\gamma_S} = 2\cos\frac{\Psi_s}{2} \quad (3)$$

The determination of materials structures in polycrystals ceramics with high surface area are being facilited microscopy techniques [13–15]. The liquid phase formed during sintering process is found by means of determination of dihedral angle [16, 17].

Under appropriate experimental conditions, surface dihedral angles, relative grain boundary energies, and surface diffusivities determined from Atomic Force Microscopic (AFM) measurements are consistent with data acquired by more laborious techniques [13].

The densification equations for pressure less solid state sintering can be easily extended to describe the densification behavior during hot-pressing or hot-isostatic-pressing [18, 19].

In this paper the use of the AFM technique to determine the dihedral surface angle for compacts sintered in solid-phase with anisotropic grain growth of 0.5 mol% MnO_2-doped tin dioxide obtained by the chemical method of the polymeric precursor is described.

Experimental procedure

The polymeric precursor solution was prepared by the Pechini method, which has been used to synthesize polycationic powders [20–28]. The process is based on the metallic citrate polymerization using ethylene glycol. A hydrocarboxylic acid, such as citric acid, is used to chelate cations in an aqueous solution. The addition of a glycol such as ethylene glycol leads to the formation of an organic ester. Polymerization, promoted by heating the mixture, results in a homogeneous resin in which metal ions are uniformly distributed throughout the organic matrix.

In the experiments, tin chloride dehydrated $SnCl_2 \cdot 2H_2O$ (Merck) was first dissolved in distilled water. Subsequently ammonium hydroxide—NH_4OH (Synth) was added in order to form tin hydroxide—$Sn(OH)_2$ [29], according to Eq. 4.

$$SnCl_2 + NH_4OH \rightarrow Sn(OH)_2 + NH_4Cl \quad (4)$$

The presence of chloride in the solution was analyzed after decantation by means of the addition of silver nitrate in the filtrate liquid. Due to the silver chloride formed as a white solid insoluble in water [30] it is possible to predict the absence of Cl^- within tolerance limit for the following equation.

$$Ag^+_{(aq)} + Cl^- \rightarrow AgCl_{(s)} \quad (5)$$

With the controlled addition of citric acid anhydrous—$C_6H_8O_7$, dissolved at 50 °C for 1 h, the formation of tin citrate took place. The citric acid/metal molar ratio was fixed at 3:1.

Manganese acetate (Carlo Erba) was added at 0.5 mol% to obtain the doped compositions 0.5 mol% MnO_2-doped tin dioxide. The polymerization occurred upon the addition of ethylene glycol—$C_2H_6O_2$. The mass ratio of the citric acid/ethylene glycol was set at 60:40.

This mixture was then stirred at 80 °C for 1 h until the solution became completely transparent. This solution was further heated at 130 °C to promote polymerization and remove excess solvents.

The powder obtained was heat-treated in an oxygen atmosphere at 400 °C for 4 h, in order to oxidate the remaining organic matter. The powder obtained in this way is referred to as the ''precursor''. In the furnace, the precursor was heat-treated at the 600 °C during 15 h, in an Al_2O_3 boat, and then cooled to room temperature.

This obtained powder was compacted by uniaxial pressing (SCHWING SIWA-15T) using pressure of 15 MPa followed by isostatic pressing (CARLZEISS-JENA) using pressure of 210 MPa forming cylindrical disks of approximately 6.0 mm of diameter and 6.0 mm of height, where the green density reached 60% of the theoretical density. The sintering process was performed in a dilatometer (NETZSCH 402E) using a constant heating rate of 2.5 °C/min under atmosphere of synthetic air, reaching the final temperature of 1,350 °C and soak time ranging from 30–120 min.

The disks of sintered 0.5 mol% MnO_2-doped tin dioxide were observed by Transmission Electronic Microscopy (TEM) employing a Philips CM200 equipment.

A standard procedure for TEM sample preparation starting from bulk samples which included cutting, grinding and dimpling was used.

Atomic force microscopy (AFM) was used to obtain an accurate analysis of the sample surface and the quantification of very important parameters such as roughness and average grain size. A Digital Instruments Multimode Nanoscope IIIa (Santa Barbara, CA) was used. AFM imaging was carried out in the contact mode, using a triangular-shaped 200-μm long cantilever with a spring constant of 0.06 N/m.

Results

The curves of linear shrinkage and shrinkage rate are depicted in the Fig. 1. By means of this analysis it was

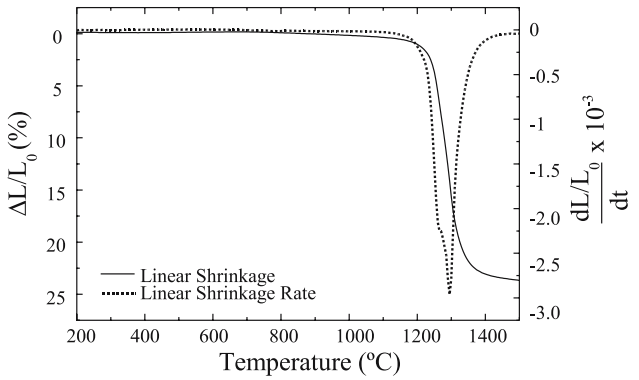

Fig. 1 Linear shrinkage and shrinkage rate of the sintered 0.5 mol% MnO_2-doped tin dioxide samples

possible to verify that the 0.5 mol% manganese doping in tin dioxide is a sufficient amount to obtain sintered samples with densification closer to theoretical densitiy (25%). The derivative of the curve represents a sintering in solid phase without chemical substance transformation.

The sintered tin dioxide tend to form an equilibrium angle of 120° in the bulk interior due to the vectorial action of the resultants in agreement with the micrograph of transmission electronic microscopy of the Fig. 2.

By means of atomic force microscopy (AFM) an accurate analysis of the interaction among the grains, surface roughness and porosity was obtained, according to Fig 3.

Data of dihedral angles was obtained by means of AFM using procedures of section analysis, according to Fig. 4. An imaginary line is inserted under the micrograph by means of a cursor (indicated by an arrow in the Fig. 4a). The porosity and dihedral angles are determined when the

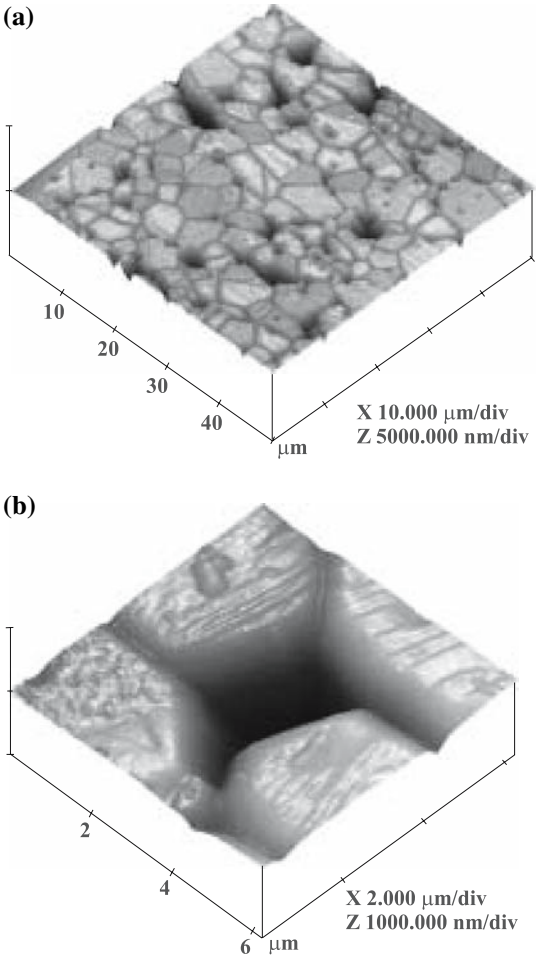

Fig. 3 AFM micrographs of the sintered 0.5 mol% MnO_2-doped tin dioxide samples. Soak time of (**a**) 30 min, (**b**) 50 min, indicating the pore detail

Fig. 2 Micrograph of transmission electronic microscopy of sintered sample of 0.5 mol% MnO_2-doped tin dioxide

cursor moves along the line. The dihedral angle was determined by extracting and adding, two adjacent angles were subtracted from 180°.

In this way, the obtained dihedral angles are of statistic significance. An average of 300 angles per sample was considered in order to obtain a more precision value (±2.1°). Thus, the dihedral angles are changed when the soak time is raised, in accordance with Fig. 5.

With the soak time ranging from 30 up to 120 min, the angle is decreased from 145° to 129°. However, the angle remain practically constant around 129.22° (±1.38°) for thermal treatment with soak times higher than 60 min. In this way, the dihedral equilibrium angle was determined.

This process is due to the migration of the manganese to the surface of tin dioxide caused by the higher temperature of thermal treatment. The exudation causes disequilibrium in the vectorial composition among the interfaces energy.

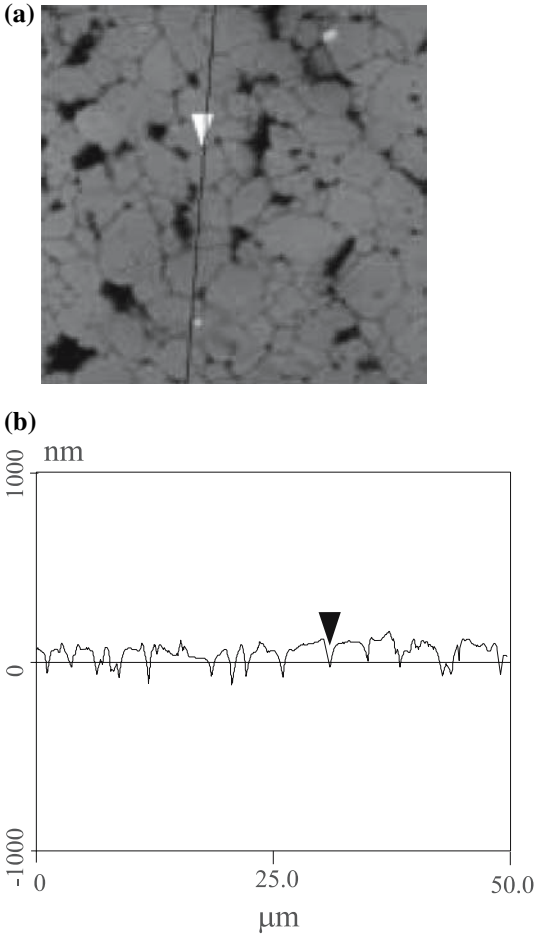

Fig. 4 Determination of dihedral angle and porosity by AFM. (**a**) Micrograph with imaginary line and lecture cursor represented by an arrow. (**b**) Representation of the cross-section attained by the cursor

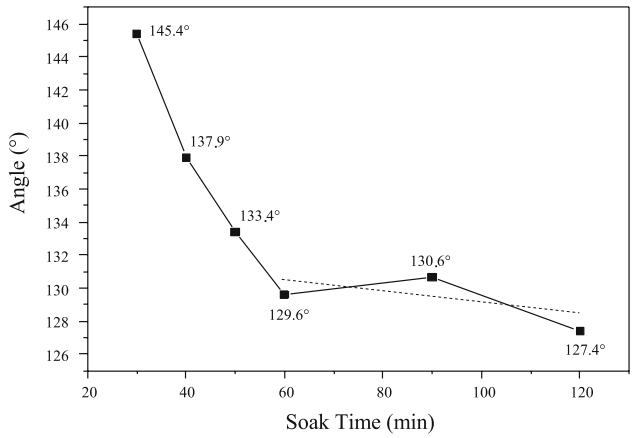

Fig. 5 Angular evolution according to the time required to reach the equilibrium angle. $SnO_2 \cdot 0.5$ mol% MnO_2. AFM Dihedral angle Thermal treatment. Er = ±1.38. FFT linear = 129.22°

Consequently, the chemical potential of SnO_2 grain boundaries is reduced as a attempt to return at the equilibrium.

The equilibrium of the grain growth in the surface is attained through thermal treatment with soak time higher than 60 min. This process is named as equilibrium dihedral angle.

Table 1 shows the number of times (fraction) that the dihedrals angles was extracted from AFM micrographs in function of the values of those angles and, for each thermal treatment. The angles were counted at each 10° starting from 90° up to 160°. In this way, the frequency in each angular interval was determined.

Figure 6 was plotted from results of Table 1 by means of Gaussian fitting. In this plot, the angular fraction appearances (in percentage) is a function of the angular intervals obtained by AFM micrographs.

A displacement of the plots was made in order to verify the effect of manganese migration into the SnO_2 surface. Thus, the maximum point of each plot was moved to a same point related to the angles axis to evaluate the width at half maximum of each plot. Such width is reduced when the time of thermal attack is increased, in accordance with the Table 2. Consequently, the manganese exudation is more effective and the SnO_2 dihedral surface angles became more uniforms along the whole analyzed surface for samples heat treated with soak times higher than 60 min.

Thus, by means of Fig. 6 it is possible to observe that the manganese is moved to surface in a homogeneous way related to the time of thermal attack. Furthermore, the appearing frequency of the SnO_2 dihedral angles in the surface is also related to the time and temperature.

Conclusion

The tin dioxide doped with a densifier agent, such as MnO_2, has a high energy gradient in the external surface when sintered. The observed grain growth is an indicative that the surface is affected by the thermal treatment. SEM micrographs showed the manganese exudation effect on the surface when the sample was heated at optimized conditions. This manganese migration at the surface led to a new grain growth in the extenal surface of the sample due to the gradient in the potential energy surface. The temperature influenced by the dynamic geometry of the oxide surface was characterized by AFM analysis. Also, this is true for anisotropic grain growth, such as in this case of SnO_2. This grain growth originated in the oxide surface is only stopped when a new angular equilibrium is stablished. In this way, a relationship between time of thermal attack and formation of a new surface equilibrium can be obtained. This process is named as equilibrium dihedral angle.

Table 1 Angular fraction corresponding for the soak times

Angle (°)	Soak time (min)					
	30	40	50	60	90	120
90°	3%	3%	2%	2%	0%	2%
100°	3%	3%	3%	3%	1%	3%
110°	3%	3%	8%	8%	8%	8%
120°	6%	5%	19%	19%	22%	23%
130°	24%	16%	29%	29%	31%	33%
140°	38%	33%	25%	24%	25%	21%
150°	19%	27%	11%	11%	10%	6%
160°	4%	10%	3%	4%	3%	4%

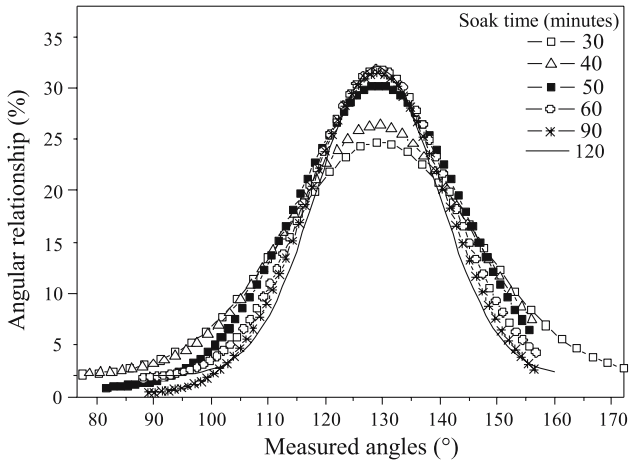

Fig. 6 Gaussian curve of the angular proportion according to the dihedral angles values

Table 2 Angular difference of width at half maximum related to the soak time

Soak time (min)	Width at half maximum
30	33°
40	27.3°
50	28.3°
60	24.9°
90	24°
120	24.3°

Acknowledgements The authors gratefully acknowledge the financial support of the Brazilian financing agencies PIBIC/CNPq and Paraná Tecnologia.

References

1. Jin MX, Shimada E, Ikuma Y (2000) J Ceram Soc Jpn 108:456
2. Kinderlehrer D, Ta'asan S, Livshits I, Mason DE (2002) Interface Sci 10:233
3. Xin TH, Wong H (2003) Acta Mater 51:2305
4. Herring C (1951) The physics of powder metallurgy. McGraw-Hill
5. Herring C (1950) J Appl Phys 21:301
6. Hansen JD, Rusin RP, Teng MH, Johnson DL (1992) J Am Ceram Soc 75:1129
7. Moment RL, Gordon RB (1964) J Am Ceram Soc 47:570
8. Readey DW, Jech RE (1968) J Am Ceram Soc 51:201
9. Shackelford JF, Scott WD (1968) J Am Ceram Soc 51:688
10. Wolf D (1983) Advances in ceramics. Americam Ceramic Society, Columbus, OH, pp 36–43
11. Dhalenne G, Dechamps M, Revcolevschi A (1983) Advances in ceramics. Americam Ceramic Society, Columbus, OH, pp 139–150
12. Kingery WD (1994) J Am Ceram Soc 77:349
13. Saylor DM, Rohrer GS (1999) J Am Ceram Soc 82:1529
14. Munoz NE, Gilliss SR, Carter CB (2004) Surf Sci 573:391
15. Saylor DM, Mason DE, Rohrer GS (2000) J Am Ceram Soc 83:1226
16. Belousov VV (2004) Colloid J 66:121
17. Belousov VV (2003) Inorg Mater 39:82
18. Shi JL (1999) J Mater Sci 34:3801
19. Beeman ML, Kohlstedt DL (1993) J Geophys Res-Solid Earth 98:6443
20. Cassia-Santos MR, Souza AG, Soledade LEB, Varela JA, Longo E (2005) J Therm Anal Calorim 79:415
21. de Lucena PR, Pessoa-Netob OD, dos Santos IMG, Souza AG, Longo E, Varela JA (2005) J Alloy Compd 397:255
22. Simoes AZ, Ramirez MA, Perruci NA, Riccardi CS, Longo E, Varela JA (2005a) Appl Phys Lett 86:112909
23. Simoes AZ, Ramirez MA, Riccardi CS, Ries A, Longo E, Varela JA (2005b) Mater Chem Phys 92:373
24. Simoes AZ, Ries A, Moura F, Riccardi CS, Longo E, Varela JA (2005c) Mater Lett 59:2759
25. Gonzalez AHM, Simoes AZ, Zaghete MA, Longo E, Varela JA (2004) J Electroceram 13:353
26. Cava S, Tebcherani SM, Pianaro SA, Paskocimas CA, Longo E, Varela J (2006) Materials Chemistry and Physics 97:102
27. Pontes FM, Leite ER, Nunes MSJ, Pontes DSL, Longo E, Magnani R, Pizani PS, Varela JA (2004) J European Ceram Soc 24:2969
28. Simoes AZ, Gonzalez AHM, Riccardi CS, Souza EC, Moura F, Zaghete MA, Longo E, Varela JA (2004) J Electroceram 13:65
29. Besso M, US Patent No 3123120:19-10-65
30. Baccan N, Aleixo L, Stein E, Godinho O (1990) Introduction to the qualitative semi micro analysis, 3rd ed. Unicamp, Campinas